Kent Academic Repository

Article

Characterisation of phosphate coacervates for potential biomedical applications

David M Pickup[1], Robert J Newport[1], Emma R Barney[2], Ji-Yung Kim[3], Sabeel P Valappil[4] and Jonathan C Knowles[5]

Abstract
In this study, amorphous $(Na_2O)_x(CaO)_{0.50-x}(P_2O_5)_{0.50} \cdot yH_2O$ (where $x = \sim 0.15$ and $y = \sim 3$) samples were prepared by a coacervate method. Thermal analysis showed that two types of water molecules were present in the coacervate structures: one type loosely bound and the other part of the phosphate structure. Structural studies using Fourier transform infrared spectroscopy (FTIR) and X-ray total diffraction revealed the samples to have very similar structures to melt-quenched glasses of comparable composition. Furthermore, no significant structural differences were observed between samples prepared using calcium nitrate as the calcium source or those prepared from calcium chloride. A sample containing ~ 1 mol% Ag_2O was prepared to test the hypothesis that calcium phosphate coacervate materials could be used as delivery agents for antibacterial ions. This sample exhibited significant antibacterial activity against the bacterium *Psuedomonas aeruginosa*. FTIR data revealed the silver-doped sample to be structurally akin to the analogous silver-free sample.

Keywords
Coacervates, phosphate glasses, biomaterials, antibacterial, FTIR, X-ray total diffraction

Introduction

Phosphate-based glasses (PBGs) containing calcium and sodium have properties that lend them to biomedical applications.[1] Glasses containing high calcium content can support both osteoblasts and fibroblasts making them suitable scaffold materials for engineering the hard/soft tissue interface.[2] Furthermore, PBGs are bioresorbable, allowing for the incorporation and release of active ions at a rate controlled by the overall dissolution rate of the glass. By fine tuning the composition the release rate may be tailored to be linear with time.[3] As a consequence, PBGs have been extensively studied over recent years for use in controlled delivery devices. PBGs containing Cu, Ag and Ga ions have been investigated as antimicrobial agents; demonstrating activity against multiresistant nosocomial pathogens and bacteria residing in biofilms.[4–6] Other related applications include oral healthcare, via the release of fluoride ions, and veterinary treatment where glasses are designed to reside in the animals' stomachs and release trace elements slowly over extended periods of time.[3] Finally, PBG can be prepared as fibres suitable for soft tissue engineering applications, where the tissue has a high degree of anisotropy.

Examples include muscle, ligaments, tendons and, potentially, nerve cells.[7]

In relation to biomedical applications, there are significant advantages to be gained by preparing PBG by low-temperature routes. For example, such methods allow for the inclusion of a wide range of drugs for controlled-release applications (e.g. Ref. [8]) and also offer the possibility to produce antibacterial, bioresorbable coatings on implant devices. The coacervate method provides an attractive alternative to the sol–gel methods

[1]School of Physical Sciences, Ingram Building, University of Kent, Canterbury, Kent, UK
[2]Electrical Systems and Optics Research Division, Faculty of Engineering, University of Nottingham, Nottingham, UK
[3]WCU Research Centre of Nanobiomedical Science, Dankook University, Dongnam-gu, Cheonan-si, Chungnam, South Korea
[4]Department of Health Services Research and School of Dentistry, University of Liverpool, Research Wing, Liverpool, UK
[5]Division of Biomaterials and Tissue Engineering, UCL Eastman Dental Institute, London, UK

Corresponding author:
David M Pickup, School of Physical Sciences, Ingram Building, University of Kent, Canterbury, Kent CT2 7NH, UK.
Email: dmp@kent.ac.uk

presently employed to prepare PBG where heating to a temperature of 250–400°C is required to drive off organic molecules and consolidate the phosphate network.[9,10]

The coacervation process is well-known.[11–14] In general, the coacervation process involves the liquid–liquid phase separation of a homogeneous solution of charged macromolecules resulting in a dense, polymer-rich 'coacervate' phase which coexists with its supernatant. In relation to PBG, the process entails the addition of a solution of polyvalent cations to a concentrated solution of sodium polyphosphate (Graham salt).[11–13,15–17] Graham salt is a water soluble polyphosphate composed of long metaphosphate chains.[18] When in solution, electrostatic interactions between the long polyphosphate chains and polyvalent cations lead to the formation of the dense coacervate phase.[17,19] The coacervate phase can be extracted and dried to form a solid glassy material. The low-temperature nature of the coacervation process, where solid samples can be produced without heating above room temperature, facilitates many applications in the preparation of PBG. These include the preparation of coatings,[20] luminescent glasses[17] and organic–inorganic hybrids for optical applications.[19] Further to this, phosphate coacervates have found a wide range of other applications including the anticorrosion protection of metals and the immobilisation of asbestos.[12]

There have been several structural studies of phosphate coacervate derived materials. Spectroscopic characterisation of a hybrid material of calcium polyphosphate and croconate ions was performed by de Oliveira et al.[19] The results revealed a structure based on helical chains of polyphosphate ions with the calcium ions occupying sites within the chains and the croconate ions on the outside hydrogen bonded to water molecules. Dias Filho et al. studied the interactions between metaphosphate chains and Ca^{2+} and Eu^{3+} cations in aqueous solution using Eu^{3+} luminescent measurements, and infrared and ^{31}P nuclear magnetic resonance (NMR) spectroscopies.[12] Their results revealed that the cations occupy two types of sites: cage-like sites within the polyphosphate chains and sites outside the chains which only become occupied once all the cage-like sites are taken. The authors concluded that it is the occupation of the second type of site that leads to supramolecular interactions between the chains that result in the formation of the coacervate. These findings are supported by the results of a study of Ni^+ and Co^{2+} containing phosphate coacervates using X-ray absorption and Raman spectroscopies.[13] A recent study of manganese polyphosphates containing azo dyes using luminescence, Raman and reflectance spectroscopies showed that the Mn^{2+} ions reside within a hydrated phosphate structure.[17]

The work also demonstrated that the incorporated dyes were pH sensitive and could be released into aqueous media. All these studies indicate that cations provide the cross-linking between phosphate chains, but only when present in quantities greater than that required to occupy all the preferred intrachain sites.

In this paper, we report the preparation and characterisation of PBG coacervates containing Na^+ and Ca^{2+} ions for potential biomedical applications. In order to demonstrate an application of these materials in this field, we prepared one sample containing silver ions and measured its antibacterial activity. The samples were characterised using thermal analysis, infrared spectroscopy and X-ray total diffraction (XRTD). To our knowledge, this is the first XRTD study of a coacervate-derived phosphate glass.

Materials and methods

Sample preparation

The following reagents were used in the preparation of the coacervate samples: sodium polyphosphate $((Na(PO_3))_n$, Sigma-Aldrich, 96%) calcium nitrate $(CaNO_3 \cdot 4H_2O$, Fisher, >99%), calcium chloride $(CaCl_2$, Sigma-Aldrich, 96%) and silver nitrate $(AgNO_3$, Sigma-Aldrich, >99%).

The samples were prepared by slowly adding a 2 M solution of the calcium salt to an equal volume of a 4 M solution of sodium polyphosphate at a rate of 5 ml/h using a syringe pump. The sodium polyphosphate solution was stirred during this addition and the resultant mixture stirred for a further hour after the addition was complete to ensure homogeneity. The stirring was then stopped and the mixture allowed to stand for 1 h. During this time two layers formed: an aqueous layer and a 'coacervate' layer. The coacervate layer was twice washed with deionised water before leaving to stand overnight. After removal of the water layer, a clear, viscous coacervate remained. The coacervate layer was dried at room temperature in a vacuum desiccator containing silica gel for several days to produce a friable powder. Typically, 5 ml of sodium polyphosphate solution yielded 1 g of PBG. This preparation is summarised in Figure 1.

Three coacervate samples were prepared and characterised. Two Na_2O-CaO-P_2O_5 glasses were prepared, one using $CaNO_3 \cdot 4H_2O$ as the calcium precursor and the other using $CaCl_2$. Hereafter, these samples will be referred to as COA1 and COA2, respectively. A third sample was prepared to nominally contain 1 mol% Ag_2O by the addition of 1 M $AgNO_3$ solution to the coacervate before drying. This silver-doped sample will be referred to as COA3.
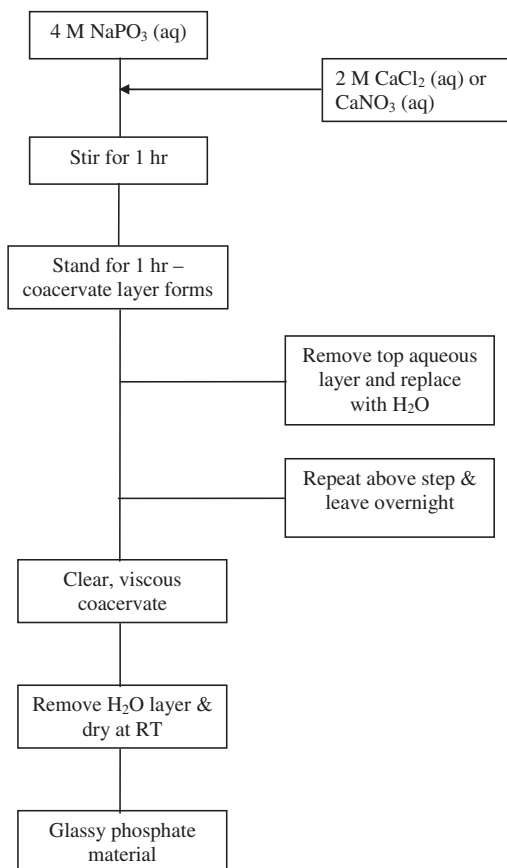
Figure 1. General schematic for the preparation of coacervate derived phosphate glasses.

The compositions of the COA1 and COA2 samples were determined by energy dispersive X-ray spectroscopy (EDS). Samples were coated with carbon by vapour deposition and viewed on a Jeol scanning electron microscope (JSM 5500 LV). Elemental analyses were performed using an Oxford Instruments Inca 400 EDS detector.

Thermal analysis

Simultaneous thermogravimetric (TG) and differential thermal analysis (DTA) of the COA1 and COA2 samples was carried out on a Setaram Labsys^{TM} TG-DTA16 instrument. The samples were heated at a rate of 5°C min^{-1} from 40 to 1000°C under air. The data were corrected by subtracting traces recorded from an empty crucible. A further sloping background was subtracted from the DTA traces in order render the peaks clearly visible.

Density measurements

The density measurements were made using a Micromeritics® Accupyc1340 pycnometer, which utilizes Archimedes' Principle using helium gas as the fluid.

Fourier transform infrared spectroscopy (FTIR)

The FTIR data were collected on a Thermo Nicolet 380 FT-IR spectrometer fitted with a diamond-anvil attenuated total reflectance (ATR) attachment. Spectra were recorded over the range 4000–400 cm^{-1} with a resolution of 1 cm^{-1} and each composed of 256 summed scans. Along with data from the dried coacervate samples, FTIR spectra were recorded from $(CaO)_{0.5}(P_2O_5)_{0.5}$ and $(CaO)_{0.4}(Na_2O)_{0.1}(P_2O_5)_{0.5}$ metaphosphate glasses for comparison. These latter samples were prepared by melt-quenching for a previous structural study.[21]

X-ray total diffraction

The XRTD data were collected on a Panalytical X'pert Pro Multi-Purpose Diffractometer at the Rutherford Appleton Laboratory, UK. The diffractometer was configured for the study of amorphous materials with a short-wavelength ($\lambda = 0.5609$ Å) silver-anode X-ray tube and capillary stage for sample mounting. Finely powdered samples were loaded in 1 mm diameter silica capillaries with a nominal wall thickness of 0.01 mm. Data were collected from a spinning sample for scattering angles from 3° to 156° with an interval of 0.2° using a silicon scintillation point detector. The data were corrected for background, absorption, polarization, multiple scattering and bremsstrahlung effects using the program GudrunX.[22] The resultant scattered intensity, $i(Q)$, can reveal structural information by Fourier transformation to obtain the pair-distribution function[23]:

$$T(r) = 4\pi\rho_o r + \frac{\pi}{2} \int_0^\infty Qi(Q)M(Q) \sin(Qr)d(Q) \quad (1)$$

where ρ_o is the macroscopic number density and $M(Q)$ is a Lorch modification function[24] necessitated by the finite maximum experimentally attainable value of Q.

Structural parameters were obtained from the diffraction data by modelling the Q-space data and converting the results to r-space by Fourier transformation to allow comparison with the experimentally determined correlation function.[25] The structural parameters used to generate the Q-space simulation were varied to optimise the fit to the experimental data using the program NXFit_R1.[26] The Q-space simulation was generated using the following equation:

$$p(Q)_{ij} = \frac{N_{ij}w_{ij}}{c_j} \frac{\sin QR_{ij}}{QR_{ij}} \exp\left[\frac{-Q^2\sigma_{ij}^2}{2}\right] \quad (2)$$

where $p(Q)_{ij}$ is the pair function in reciprocal space, N_{ij}, R_{ij} and σ_{ij} are the coordination number, atomic

separation and disorder parameter, respectively, of atom i with respect to j, c_j is the concentration of atom j and w_{ij} is the weighting factor. The weighting factors are given by:

$$w_{ij} = \frac{2c_i c_j f(Q)_i f(Q)_j}{\overline{f(Q)}^2} \quad \text{if } i \neq j \tag{3}$$

or

$$w_{ij} = \frac{c_i^2 f(Q)_i^2}{\overline{f(Q)}^2} \quad \text{if } i = j \tag{4}$$

where $f(Q)$ represents the Q-dependant X-ray form factors.

Previous work has shown that there is little difference in the atomic separations of Ca–O (2.34 Å) and Na–O (2.33 Å) correlations in PBG.[21] This can be understood in terms of the similar ionic radii of Ca and Na, 0.99 and 0.95 Å, respectively.[27] In this study, Ca and Na have been combined for fitting purposes into one generic metal atom, M, which has an average X-ray form factor weighted to the concentrations of the two elements.[27]

Antibacterial assay

The silver-doped coacervate glass (COA3) was investigated for its ability to inhibit bacterial growth using a disk diffusion methodology (BSAC Disk Diffusion Method for Antimicrobial Susceptibility Testing, Version 4, 2005). Isosensitest agar (Oxoid, Basingstoke, UK) plates were inoculated with a standardized culture (optical density of 0.03 at a wavelength of 600 nm) of *Psuedomonas aeruginosa* (Epidemiological strain, School of Dentistry, University of Liverpool).

One hundred milligrams of both control (COA1) and silver-doped glass powders were pressed into 5 mm diameter discs using Atlas[TM] Evacuable Pellet Dies (Specac Ltd, UK) and placed in each of the inoculated plates. The experiment was conducted in triplicate and the glass not containing any silver was used as a negative control. These plates were then incubated aerobically at 37°C for 24 h. The diameters of any zones that had formed around the samples were measured using callipers.

Results

Sample characterisation

The elemental compositions of the Na_2O-CaO-P_2O_5 samples are reported in Table 1 below. Table 2 gives these compositions expressed in terms of simple oxides. The numbers in this table were calculated by assuming that any excess oxygen is charge balanced by protons. Using the mole fractions of the oxides, the compositions of the COA1 and COA2 samples can be written as $(Na_2O)_{0.16}(CaO)_{0.36}(P_2O_5)_{0.48} \cdot 2.9H_2O$ and $(Na_2O)_{0.18}(CaO)_{0.35}(P_2O_5)_{0.47} \cdot 3.1H_2O$, respectively. The composition of the silver-doped COA3 sample was not measured.

Figure 2 shows the combined TGA/DTA traces obtained from the dried COA1 and COA2 samples.

The measured densities of the COA1 and COA2 samples are reported in Table 1.

Structural studies

The FTIR spectra of the COA1 and COA3 coacervate samples are compared to those from melt-quenched $(CaO)_{0.5}(P_2O_5)_{0.5}$ and $(CaO)_{0.4}(Na_2O)_{0.1}(P_2O_5)_{0.5}$

Table 1. Sample characterisation.

Sample	Composition (wt%)				Density (g cm^{-3})
	O	Na	P	Ca	
COA1	64.54 ± 1.07	5.04 ± 0.37	20.37 ± 0.56	10.05 ± 0.50	2.326 ± 0.010
COA2	64.95 ± 0.74	5.68 ± 0.34	19.90 ± 0.41	9.48 ± 0.24	2.281 ± 0.010

Table 2. Sample compositions expressed in terms of simple oxides.

Sample	Composition (mol%)				Composition (wt%)			
	Na_2O	CaO	P_2O_5	H_2O	Na_2O	CaO	P_2O_5	H_2O
COA1	4.03 ± 0.30	9.24 ± 0.46	12.08 ± 0.33	74.65 ± 0.65	6.52 ± 0.48	13.54 ± 0.67	44.80 ± 1.23	34.14 ± 0.58
COA2	4.45 ± 0.27	8.54 ± 0.22	11.56 ± 0.24	75.45 ± 0.46	7.34 ± 0.44	12.75 ± 0.32	43.71 ± 0.90	36.20 ± 0.41

metaphosphate glasses in Figure 3. The absorption bands have been assigned according to the literature and labelled in Figure 3. The band near $1250\,cm^{-1}$ is assigned to the asymmetric stretching mode of the two non-bridging oxygen (NBO) atoms bonded to phosphorus atoms in the PO_2 metaphosphate units, $\nu_{as}(PO_2)^{-}$.[28,29] The absorption bands close to 1100 and $1000\,cm^{-1}$ are assigned to the asymmetric and symmetric stretching modes of chain-terminating PO_3 groups ($\nu_{as}(PO_3)^{2-}$ and $\nu_{s}(PO_3)^{2-}$), respectively, although the latter assignment remains tentative.[30] The absorption band near $900\,cm^{-1}$ is assigned to the asymmetric stretching modes of the P–O–P linkages, $\nu_{as}(P–O–P)$,[31] and the partially split band centred around $750\,cm^{-1}$ is assigned to the symmetric stretching modes of these linkages, $\nu_{s}(P–O–P)$.[29] The peak at $540\,cm^{-1}$ is attributed to $O−P−O$ deformation modes.[31]

The XRTD data for the COA1 and COA2 samples are shown in Figures 4 and 5, respectively. The structural parameters obtained from the fitting of these XRTD data are shown in Table 3. It should be noted that it was not possible to collect XRTD from the

Ag-doped sample (COA3) because the X-rays used were generated by a silver-anode tube: X-ray fluorescence from the silver in the sample would have swamped the diffraction signal.

Antibacterial assay

The silver-doped sample had a growth inhibition zone of 22.5 mm with a standard deviation of 2.6 mm against *P. aeruginosa* (Liverpool hospital strain). The control did not show any growth inhibition.
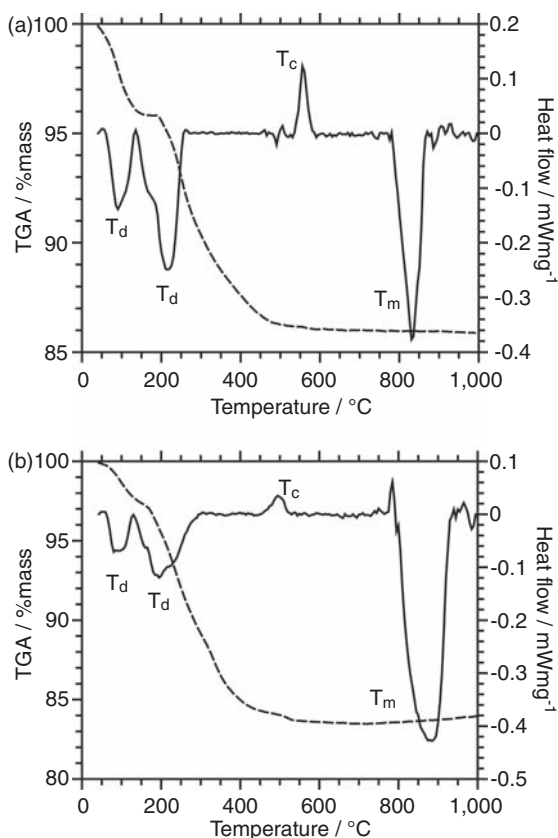
Figure 2. Simultaneous TGA (dashed lines) and DTA (solid lines) measurements from the coacervate samples: (a) COA1 and (b) COA2.
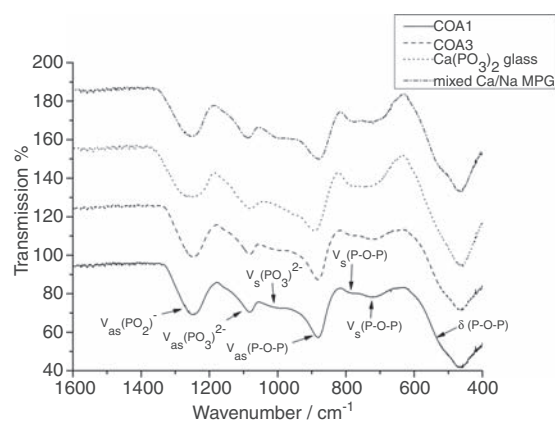
Figure 3. FTIR spectra from undoped (COA1) and silver-doped (COA3) coacervate samples compared with those from melt-quenched metaphosphate glasses. The upper three curves have been off-set for clarity. Mixed Ca/Na MPG refers to $(CaO)_{0.4}(Na_2O)_{0.1}(P_2O_5)_{0.5}$ metaphosphate glass.
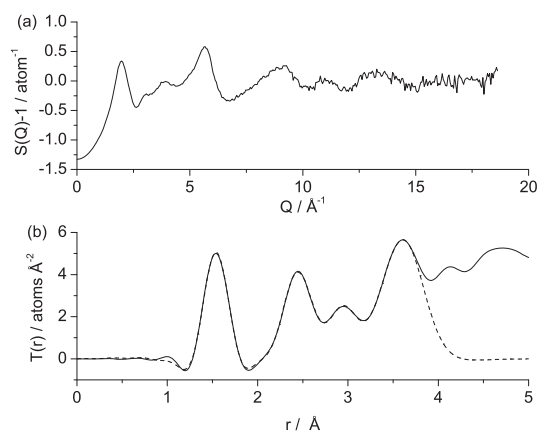
Figure 4. X-ray total diffraction data from the COA1 coacervate sample: (a) Q-space interference function and (b) real-space pair-distribution function (solid line) together with its simulation (dashed line).

Figure 5. X-ray total diffraction data from the COA2 coacervate sample: (a) Q-space interference function and (b) real-space pair-distribution function (solid line) together with its simulation (dashed line).

Table 3. Structural parameters obtained from the fitting of the XRTD data.[a]
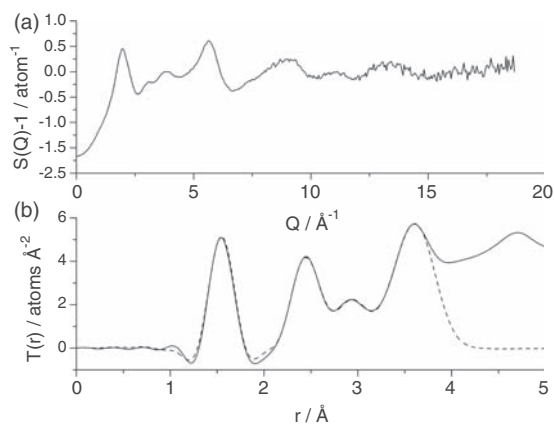
Sample	Correlation	R (Å)	c.n.	σ (Å)
COA1	P–NBO	1.51	2.3	0.03
	P–BO	1.59	1.8	0.04
	M–O	2.38	3.6	0.08
	O–O	2.54	3.5	0.11
	M–P	2.89	2.2	0.07
	P–P	2.97	1.9	0.09
COA2	P–NBO	1.52	2.3	0.03
	P–BO	1.58	1.8	0.03
	M–O	2.39	3.5	0.06
	O–O	2.54	3.4	0.11
	M–P	2.89	2.3	0.07
	P–P	2.98	1.8	0.10

[a]R is the atomic separation, c.n. the coordination number and σ the disorder parameter. M denotes the generic metal cation, BO is a bridging oxygen and NBO is a non-bridging oxygen. The errors are reasonably estimated as ± 0.02 Å in R, $\pm 15\%$ in N and ± 0.01 Å in σ.

Discussion

Sample characterisation

Figure 2 shows the TG-DTA curves obtained from the COA1 and COA2 coacervate samples. Both TGA curves exhibit two distinct regions of mass loss: a 3–5% loss between 40 and 200°C and a further 10–14% decrease between 200 and 500°C. Both of these events can be attributed to dehydration of the sample. The low-temperature mass loss is due to the removal of loosely bound water molecules from outside the polyphosphate structure[19] whereas the higher-temperature decrease in mass is due to the loss of structural water molecules.[17] Both DTA traces exhibit two endothermic peaks centred at ~95 and ~200°C that correlate well with two mass loss features in the TGA curve and are therefore ascribed to dehydration of the samples. Consequently these peaks are labelled T_d in Figure 2. The exothermic peaks (T_c) observed at 490°C for the COA1 sample and at 450°C for the COA2 are attributed to crystallization. The large endothermic peaks (T_m) at 810 and 830°C for the COA1 and COA2 samples, respectively, are due to the samples melting.

Similar TG behaviour has been observed previously for calcium polyphosphate coacervates containing croconate ions.[19] The DTA results presented here support the conclusion that there are two types of water present in the coacervate structure leading to two dehydration events, clearly visible in the TGA and DTA data. The observation of crystallization and melting events at higher temperatures in the DTA traces is consistent with the behaviour of melt-quenched PBG of similar composition over the same temperature range.[32]

Structural study

The FTIR spectra of the COA1 and COA3 samples shown in Figure 3 exhibit the absorption bands at 1250, 1100, 1000, 900, 750 and 540 cm^{-1} that are associated with polyphosphate materials.[29–31] Such materials have structures based on polyphosphate chains made up of tetrahedral PO_4 units. The polyphosphate chains are negatively charged and are held together by the electrostatic force that exists between them and any cations present.[33] These chains contain two distinct phosphorus sites: chain-terminating end groups, $(PO_3)^{2-}$, and intrachain middle groups, $(PO_2)^-$. As outlined in the results section, the vibrational spectra shown here exhibit modes associated with both phosphorus environments: the band at 1250 cm^{-1} arises from stretching of the bonds in the $(PO_2)^-$ middle groups, whereas the bands at 1100 and 1000 cm^{-1} are due to modes involving the $(PO_3)^{2-}$ end groups. The remaining bands at 900, 500 and 540 cm^{-1} are due to modes involving the P–O–P bonds that join the $(PO_2)^-$ middle groups and $(PO_3)^{2-}$ end groups together to form chains. Also, shown in Figure 3 are the vibrational spectra from two melt-quenched metaphosphate glasses of similar composition to the coacervate samples, i.e. $(CaO)_{0.5}(P_2O_5)_{0.5}$ and $(CaO)_{0.4}(Na_2O)_{0.1}(P_2O_5)_{0.5}$. The similarity between the spectra from the coacervate samples and those from the melt-quenched samples is striking: the only discernible difference is that the absorption bands in the spectra from the coacervates are slightly broader than those in the spectra from the glasses.

This perhaps reflects a greater disorder in the structures of the coacervate samples which may be due to the presence of water in the structure as evidenced by the thermal analysis. Furthermore, the similarity between the spectra from the two coacervates samples, one containing silver and the other silver-free suggests that the addition of ~1 mol% Ag_2O does not change the structure of the coacervate significantly.

As mentioned above, the coacervate samples studied here have structures consisting of polyphosphate chains with the anions (in this case Ca^{2+} and Na^+) occupying sites between chains. XRTD can yield information on the distances between atoms in these structures and their associated coordination numbers. Considering the structure of polyphosphate chains, it can be seen that there are two types of oxygen atoms present: bridging oxygens (BOs) that are bonded to two phosphorus atoms and terminal or NBOs which only connect to one phosphorus atom. Thus, the $(PO_2)^-$ middle groups and $(PO_3)^{2-}$ end groups mentioned previously have two and three NBOs, respectively: the remaining oxygen atoms that make up the PO_4 tetrahedra are BOs. The presence of two types of oxygen atom has been taken into consideration when modelling the XRTD data shown in Figures 4 and 5 by using the corresponding two correlations to fit the peak at ~1.6 Å in the pair-distribution function. The resultant structural parameters in Table 3 reflect this. The shorter correlation of 1.51 Å is ascribed to P–NBO bonds and the longer one at 1.59 Å is attributed to P–BO bonds.[34] The P-NBO bonds are shorter because their bond order is slightly greater than one. For both samples, the sum of the P-NBO and P-BO coordination numbers is very close to 4, reflecting the fact that the polyphosphate chains are made up of PO_4 tetrahedra. The fact that the P-NBO coordination numbers are slightly greater than the P-BO coordination numbers which indicates the presence of chain-termination $(PO_3)^{2-}$ as suggested by the FTIR data and demonstrates that the polyphosphate chains have a finite length (as opposed to infinite chains or rings which would contain only $(PO_2)^-$ middle groups).

The remaining structural parameters reported in Table 3 are similar to those measured previously from amorphous CaO-Na$_2$O-P$_2$O$_5$ materials.[10,21] To reduce the number of parameters in the fitting process, the data have been modelled using a generic metal cation, M, instead of distinct Na^+ and Ca^{2+} contributions. The coordination environment for the cations reported in Table 3 is consistent with a site surrounded by NBOs from the phosphate chains. The O···O distance in Table 3 represents that across an edge of the PO_4 tetrahedron and agrees well with the value of 2.52 Å that can be calculated by taking the average P–O distance to be 1.55 Å and the O–P–O angle to be 109°. The nearest-neighbour P···P distance of 2.98 Å agrees well with the

value of 2.94 Å measured from vitreous P_2O_5.[35] The P···P coordination number should be equal to the P-BO coordination number since the phosphorus atoms are connected by BOs. The results presented here exhibit good agreement between these coordination numbers.

Finally, examining the structural parameters in Table 3, it can be seen that there are no significant structural differences between the sample prepared using $CaNO_3$ as the calcium source (COA1) and that prepared from $CaCl_2$ (COA2).

Antibacterial properties

The silver-doped coacervate sample (COA3) exhibited significant antibacterial activity against *P. aeruginosa* compared to the control (COA1). The zone of inhibition of 23 mm observed in this study compares well with that of 9 mm measured in a previous study of melt-quenched PBG containing 1 mol% Ag_2O.[36] However, the larger zone of inhibition observed here cannot be directly correlated with the previous findings from Ahmed et al.[36] because of the difference in bacterial strains used (Liverpool hospital strain as opposed to the strain PA01 used by Ahmed et al.). Moreover, the preparation of the glass powder as pellets in this study could have resulted in an increased surface area and faster release of silver ions from the coacervate sample compared with the melt-derived glass of similar composition. However, the result presented here demonstrates the potential for phosphate coacervate materials to be used as a vehicle for the delivery of antibacterial ions and possibly other drug molecules.[37]

Conclusions

The results show that the coacervate method can be readily used to produce PBG materials of approximate composition $(Na_2O)_{0.15}(CaO)_{0.35}(P_2O_5)_{0.50} \cdot 3H_2O$ with structures based on phosphate chains. Structurally these materials are very similar to melt-quenched metaphosphate glasses of similar composition except for the inclusion of water. Thermal analysis of the samples suggested the presence of two water environments, one structural and one loosely bound, which is consistent with previous measurements.[19] XRTD revealed no significant differences between the structure of the sample prepared using $CaNO_3$ as the calcium source and that prepared using $CaCl_2$. Finally, the potential use of coacervate-derived phosphate glasses as biomaterials has been demonstrated by the preparation of a silver-doped sample that acts as a delivery agent for antibacterial Ag^+ ions and exhibits effectiveness at killing the bacterium *P. aeruginosa*.

Declaration of conflicting interest

None declared.

Funding

References

1. Abou Neel EA, Pickup DM, Valappil SP, et al. Bioactive functional materials: a perspective on phosphate-based glasses. *J Mater Chem* 2009; 19: 690–701.
2. Bitar M, Salih V, Mudera V, et al. Soluble phosphate glasses: in vitro studies using human cells of hard and soft tissue origin. *Biomaterials* 2004; 25: 2283–2292.
3. Knowles JC. Phosphate based glasses for biomedical applications. *J Mater Chem* 2003; 13: 2395–2401.
4. Mulligan AM, Wilson M and Knowles JC. Effect of increasing silver content in phosphate-based glasses on biofilms of Streptococcus sanguis. *J Biomed Mater Res A* 2003; 67A: 401–412.
5. Mulligan AM, Wilson M and Knowles JC. The effect of increasing copper content in phosphate-based glasses on biofilms of Streptococcus sanguis. *Biomaterials* 2003; 24: 1797–1807.
6. Valappil SP, Ready D, Abou Neel EA, et al. Antimicrobial gallium-doped phosphate-based glasses. *Adv Funct Mater* 2008; 18: 732–741.
7. Shah R, Sinanan ACM, Knowles JC, et al. Craniofacial muscle engineering using a 3-dimensional phosphate glass fibre construct. *Biomaterials* 2005; 26: 1497–1505.
8. Pickup DM, Newport RJ and Knowles JC. Sol-gel phosphate-based glass for drug delivery applications. *J Biomater Appl* 2012; 26: 613–622.
9. Carta D, Pickup DM, Knowles JC, et al. Sol-gel synthesis of the P_2O_5-CaO-Na_2O-SiO_2 system as a novel bioresorbable glass. *J Mater Chem* 2005; 15: 2134–2140.
10. Pickup DM, Guerry P, Moss RM, et al. New sol-gel synthesis of a $(CaO)_{0.3}(Na_2O)_{0.2}(P_2O_5)_{0.5}$ bioresorbable glass and its structural characterisation. *J Mater Chem* 2007; 17: 4777–4784.
11. Gomez F, Vast P, Llewellyn P, et al. Dehydroxylation mechanisms of polyphosphate glasses in relation to temperature and pressure. *J Non-Cryst Solids* 1997; 222: 415–421.
12. Dias FA, Carlos LD, Messadeq Y, et al. Spectroscopic study and local coordination of polyphosphate colloidal systems. *Langmuir* 2005; 21: 1776–1783.
13. Silva MAP, Franco DF and de Oliveira LFC. New insight on the structural trends of polyphosphate coacervation processes. *J Phys Chem A* 2008; 112: 5385–5389.
14. Kaloti M and Bohidar HB. Kinetics of coacervation transition versus nanoparticle formation in chitosan-sodium tripolyphosphate solutions. *Colloid Surf B* 2010; 81: 165–173.
15. Kanazawa T, Umegaki T, Kitajima Y, et al. Solubility study of coacervates of magnesium, calcium and aluminum high polyphosphates in acid solutions. *Bull Chem Soc Jpn* 1974; 47: 1419–1421.
16. Umegaki T, Nakayama Y and Kanazawa T. Thermal change of magnesium high polyphosphate coacervates. *Bull Chem Soc Jpn* 1976; 49: 2105–2107.
17. de Oliveira LFC, Silva MAP, Brandao AR, et al. Amorphous manganese polyphosphates: preparation, characterization and incorporation of azo dyes. *J Sol-Gel Sci Technol* 2009; 50: 158–163.
18. Casas JM, Garcia MP, Sanz M, et al. P-31 NMR spectroscopic studies of the influence of the environment in the degradation process of the Graham's salt. *Ceram Int* 2010; 36: 39–46.
19. de Oliveira CIR, de Oliveira LFC, Dias FA, et al. Spectroscopic investigation of a new hybrid glass formed by the interaction between croconate ion and calcium polyphosphate. *Spectrochim Acta Part A* 2005; 61: 2023–2028.
20. Iost A, Bigot R, Barbieux F, et al. Mechanical behavior of metaphosphate glasses used as coating on metals in relation to their structure and preparation method. *J Mater Sci* 1999; 34: 3991–3996.
21. Pickup DM, Ahmed I, Guerry P, et al. The structure of phosphate glass biomaterials from neutron diffraction and ^{31}P nuclear magnetic resonance data. *J Phys Condens Matter* 2007; 19: 415116.
22. Soper AK. GudrunX software, http://www.isis.stfc.ac.uk/support-laboratories/xrd/data-analysis/xrd-data-analysis9203.html (2013, accessed 15 May 2013).
23. Barney ER, Hannon AC, Senkov ON, et al. A neutron and X-ray diffraction study of Ca-Mg-Cu metallic glasses. *Intermetallics* 2011; 19: 860–870.
24. Lorch E. Neutron diffraction by germania silica and radiation-damaged silica glasses. *J Phys C Solid State Phys* 1969; 2: 229.
25. Gaskell PH. Glasses and amorphous materials. In: Zarzycki J (ed.) *Materials science and technology*. Vol 9, Weinheim: VCH, 1991, pp.174–278.
26. Moss RM. *Structural studies of metal doped phosphate glasses and computational developments in diffraction analysis*. PhD Thesis, University of Kent, UK, 2009.
27. Moss RM, Abou Neel EA, Pickup DM, et al. The effect of zinc and titanium on the structure of calcium-sodium phosphate based glass. *J Non-Cryst Solids* 2010; 356: 1319–1324.
28. Uchino T and Yoko T. Structure and vibrational properties of alkali phosphate glasses from ab initio molecular orbital calculations. *J Non-Cryst Solids* 2000; 263: 180–188.
29. Rouse GB, Miller PJ and Risen WM. Mixed alkali glass spectra and structure. *J Non-Cryst Solids* 1978; 28: 193–207.
30. Byun JO, Kim BH, Hong KS, et al. Properties and structure of RO-Na_2O-Al_2O_3-P_2O_5 (R=Mg, Ca, Sr, Ba) glasses. *J Non-Cryst Solids* 1995; 190: 288–295.
31. Hudgens JJ and Martin SW. Glass-transition and infrared-spectra of low-alkali, anhydrous lithium phosphate-glasses. *J Am Ceram Soc* 1993; 76: 1691–1696.

32. Ahmed I, Lewis M, Olsen I and Knowles JC. Phosphate glasses for tissue engineering: part 1. Processing and characterisation of a ternary-based P_2O_5-CaO-Na_2O glass system. *Biomaterials* 2004; 25: 491–499.
33. Brow RK. Review: the structure of simple phosphate glasses. *J Non-Cryst Solids* 2000; 263: 1–28.
34. Hoppe U. A structural model for phosphate glasses. *J Non-Cryst Solids* 1996; 195: 138–147.
35. Hoppe U, Walter G, Kranold R, et al. X-ray diffraction study of the structure of vitreous P_2O_5. *Z Naturforsch A Phys Sci* 1998; 53: 93–104.
36. Ahmed I, Ready D, Wilson M, et al. Antimicrobial effect of silver-doped phosphate-based glasses. *J Biomed Mater Res A* 2006; 79A: 618–626.
37. Dion A, Berno B, Hall G, et al. The effect of processing on the structural characteristics of vancomycin-loaded amorphous calcium phosphate matrices. *Biomaterials* 2005; 26: 4486–4494.